Published OnlineFirst September 10, 2015; DOI: 10.1158/0008-5472.CAN-15-0439

Therapeutics, Targets, and Chemical Biology

Cancer Research

Targeting the MDM2/MDM4 Interaction Interface as a Promising Approach for p53 Reactivation Therapy

Marsha Pellegrino[1], Francesca Mancini[1,2], Rossella Lucà[1], Alice Coletti[3], Nicola Giacchè[3], Isabella Manni[4], Ivan Arisi[5], Fulvio Florenzano[5], Emanuela Teveroni[1,2], Marianna Buttarelli[1], Laura Fici[1], Rossella Brandi[5], Tiziana Bruno[4], Maurizio Fanciulli[4], Mara D'Onofrio[5], Giulia Piaggio[4], Roberto Pellicciari[3], Alfredo Pontecorvi[2], Jean Christophe Marine[6,7], Antonio Macchiarulo[3], and Fabiola Moretti[1]

Abstract

Restoration of wild-type p53 tumor suppressor function has emerged as an attractive anticancer strategy. Therapeutics targeting the two p53-negative regulators, MDM2 and MDM4, have been developed, but most agents selectively target the ability of only one of these molecules to interact with p53, leaving the other free to operate. Therefore, we developed a method that targets the activity of MDM2 and MDM4 simultaneously based on recent studies indicating that formation of MDM2/MDM4 heterodimer complexes are required for efficient inactivation of p53 function. Using computational and mutagenesis analyses of the heterodimer binding interface, we identified a peptide that mimics the MDM4 C-terminus, competes with endogenous MDM4 for MDM2 binding, and activates p53 function. This peptide induces p53-dependent apoptosis *in vitro* and reduces tumor growth *in vivo*. Interestingly, interfering with the MDM2/MDM4 heterodimer specifically activates a p53-dependent oxidative stress response. Consistently, distinct subcellular pools of MDM2/MDM4 complexes were differentially sensitive to the peptide; nuclear MDM2/MDM4 complexes were particularly highly susceptible to the peptide-displacement activity. Taken together, these data identify the MDM2/MDM4 interaction interface as a valuable molecular target for therapeutic reactivation of p53 oncosuppressive function. *Cancer Res; 75(21); 4560–72. ©2015 AACR.*

Introduction

Discovery of new molecular targets for cancer therapy is a field in which considerable efforts are being employed, to develop new and safe therapeutic agents. The p53 pathway is an attractive target because of its well-documented oncosuppressive function (1, 2). Since the discovery of MDM2 as crucial p53 inhibitor (3, 4), there have been numerous attempts to pharmacologically disrupt the interaction between these two proteins to reactivate p53 in human wild-type TP53 tumors (2). This has led to the development of different classes of molecules that efficiently and specifically interfere with the formation of the MDM2/p53 complexes (i.e., Nutlin; refs. 5–7). Although p53 reactivation is observed in many wild-type TP53 cancer cells exposed to these molecules, only few of them die by apoptosis (7, 8).

The presence of MDM4 (or MDMX; ref. 9), the MDM2 homolog, has provided a rational explanation for the relatively modest p53-dependent apoptotic response observed in these cells (10–12). Indeed, computational and molecular studies provided evidence that the p53 binding domain of MDM2 and MDM4 are sufficiently dissimilar to explain the lack of activity of the MDM2 inhibitors towards MDM4 (13–15).

Importantly, these data confirmed previous genetic evidence that optimal p53 reactivation can only be achieved by targeting both MDM proteins simultaneously (16) and therefore highlighted the need of identifying molecules that target both the p53–MDM2 and p53–MDM4 interactions. Therefore, new efforts have been developed to find out new molecules able to dissociate MDM2 and MDM4 from p53 (2, 17).

Recent genetic evidence indicates that efficient inhibition of p53 requires the formation of MDM2/MDM4 heterodimers. The heterodimers are more efficient than the MDM2 homodimers in promoting ubiquitination and degradation of p53 (18, 19). Heterodimers also efficiently control basal p53 transcriptional activity *in vivo*, and thus even in the absence of MDM2 E3-ubiquitin ligase activity (20). In line with these data, MDM2 and MDM4 have been found together with p53 at the promoter of some p53 target genes to inhibit its transactivation activity (21). To further support this model, mice that express MDM4 mutants

[1]Institute of Cell Biology and Neurobiology, CNR, Roma, Italy. [2]Institute of Medical Pathology, Catholic University of Roma, Roma, Italy. [3]Department of Pharmaceutical Sciences, University of Perugia, Perugia, Italy. [4]Regina Elena Cancer Institute, Roma, Italy. [5]European Brain Research Institute (EBRI) Rita Levi-Montalcini, Roma, Italy. [6]Center for Human Genetics, KU-Leuven, Leuven, Belgium. [7]Center for the Biology of Disease, VIB, Leuven, Belgium.

Note: Supplementary data for this article are available at Cancer Research Online (http://cancerres.aacrjournals.org/).

Accession Codes: Series record GSE62855.

Corresponding Author: Fabiola Moretti, Institute of Cell Biology and Neurobiology, National Research Council of Italy (CNR), Via del Fosso di Fiorano, 64, Roma 00143, Italy. Phone: 3906-50170-3242; Fax: 3906-50170-3304; E-mail: fabiola.moretti@cnr.it

doi: 10.1158/0008-5472.CAN-15-0439

Published OnlineFirst September 10, 2015; DOI: 10.1158/0008-5472.CAN-15-0439

defective in MDM2 binding die during embryonic development (22, 23). These genetic experiments support the view that the heterodimer is required for proper control of p53 activity.

These data have raised the hypothesis that an alternative therapeutic approach for p53 reactivation in tumors is to target the interaction between MDM2 and MDM4 (18, 20). As the ubiquitin ligase activity of the heterodimers depends on the C-terminal RING finger domain of MDM2, and as MDM2 homodimers are still able to function as an E3 ligase (24, 25), we searched for molecules that bind MDM2 by simulating the MDM2 interaction interface of MDM4.

Materials and Methods

Peptides

Lyophilized Peptide3 (KEIQLVIKVFIA), Peptide3M (KEIQLVIKVAEA), Peptide SC3A (VQEAFKLIKIVI), and SC3B (AIKIFVKVLEIQ) (synthesized from Biosynthesis) were dissolved in 100% DMSO at a concentration of 10 mmol/L. Peptides purity level was $\geq$ 96%. Peptides' solution was freshly prepared at a concentration of 0.5 mmol/L in sterile distilled deionized H_2O. Peptides were premixed with growth media at 37°C for 15 minutes before addition to the cells. All peptides were used at 10 μmol/L concentration unless differently specified. All peptides were chemically modified by a capping acetyl group at the NH2- and an amide group at the C-terminus.

Computational methods

Starting from the crystal structure of the heterodimer complex (pdb code: 2VJF; ref. 19), one complex of Pep3 with MDM2 was generated shortening the RING domain of MDM4 (chain B) from residue E428 to K478, while keeping the RING domain of MDM2 (chain A). Pep3M was obtained editing the structure of Pep3 by mutating residues F488 and I489 into alanine and glutamate, respectively. The geometry of the resulting two complexes was optimized using the Protein Preparation Wizard tool as implemented in Maestro v.9.7. (Schrödinger, LLC). Two molecular systems were then prepared inserting Pep3/MDM2 and Pep3M/MDM2 complexes into a cubic box containing TIP3P water molecules for protein solvation, and extended 10 Å away from any protein atom. Each of the systems was neutralized by adding sodium and chlorine ions at a concentration of 0.15 mol/L. Periodic boundary conditions were applied to avoid finite-size effects. Molecular dynamics (MD) simulations were performed using Desmond v.3.0 and the OPLS-2005 force field. The simulation protocol included an initial energy minimization over a maximum of 2,000 steps, with a convergence criterion of 50 kcal/mol/Å, and the presence of harmonic restraints on the solute atoms (force constant = 50.0 kcal/mol/Å2); a second energy minimization without restraints; a third stage of 12 picoseconds (ps) at 10 K with harmonic restraints on the solute heavy atoms (force constant = 50.0 kcal/mol/Å2), using the NVT ensemble and Berendsen thermostat; a fourth 12 ps at 10 K, retaining the harmonic restraints, and using the NPT ensemble and Berendsen thermostat and barostat; a fifth heating phase of 24 ps at 300 K, retaining the harmonic restraints, and using the NPT ensemble and Berendsen thermostat and barostat; a final 24 ps at 300 K without harmonic restraints, using the NPT Berendsen thermostat and barostat. The final production phase of 30 nanoseconds (ns) was run using the canonical NPT Berendsen ensemble at temperature 300 K. During MD simulations, a time step of 2 femtoseconds (fs) was used inserting constrains on the bond lengths of hydrogen atoms with the M-SHAKE algorithm (26). A total of 6252 frames of atomic coordinates were saved along the MD trajectories. The occupancy of intermolecular hydrogen bonds between Pep3, Pep3M, and MDM2 was calculated using a cut-off value of 10%.

Cell cultures and treatments

Human primary fibroblasts, MCF7, $p53^{+/+}$ and $p53^{-/-}$HCT116, HepG2, and H1299 cells were maintained in DMEM, GTL-16 in RPMI supplemented with 10% FBS (Gibco). MCF7, HCT116, and GTL-16 cell identity has been confirmed by PowerPlex 18D System (Promega) by BMR Genomics service (last analysis December 2013). Mycoplasma-free conditions have been routinely tested by MycoAlert kit (Lonza). MCF10A cells were maintained in MEBM supplemented with specific condiments according to the manufacturer's instructions (Lonza). $p53^{-/-}Mdm2^{-/-}Mdm4^{-/-}$MEFs (TKO-MEF) were maintained in DMEM high glucose supplemented with 10% FBS (FBS-Cambrex). Transient transfections were performed by Lipofectamine Plus reagent (Life Sciences) according to the manufacturer's instructions. All stealth siRNAs are from Life Technologies. MDM2 and MDM4 mutants were generated by QuikChange XL Site-Directed Mutagenesis Kit according to the manufacturer's instructions (Stratagene).

Imaging

Imaging was performed through a confocal laser scanning microscope (Leica SP5, Leica Microsystems) equipped with four laser lines and a transmitted light detector for differential interference contrast (Nomarski) imaging. The following acquisition settings were used: objective 63× oil immersion NA 1.4; zoom factor 2; image format 1024×1024; sampled image area was *x*: 122 μm, *y*: 122 μm; pinhole 1 producing an optical section thickness of 0.8 μm; speed acquisition 10 Hz. A random set of single plane images of both fluorescence and bright field channels was taken to analyze the peptide cellular distribution throughout the coverslip. The confocal image acquisitions were performed so that all samples were imaged using the same settings for laser power and detector gain. Brightness and contrast of images were globally enhanced by using linear histogram correction and slightly oversaturated to allow a better qualitative visual evaluation of the morphologic features.

Viability and apoptosis analyses

For the Annexin V–propidium iodide staining, cells were collected, washed with PBS, and stained by Annexin V–FITC and propidium iodide according to the manufacturer's protocol (Clontech). Cells were analyzed by FACScan flow cytometer and data analyzed by CellQuest Software (Becton Dickinson). Cell-cycle profiles were evaluated by FACS analyses of 70% ethanol-fixed cells stained with 0.1 mg/mL propidium iodide/PBS and 2 mg/mL RNaseA solution. Apoptotic DNA fragmentation analysis was carried out by terminal deoxynucleotidyltransferase–mediated dUTP nick end labeling (TUNEL) assays with fluorescent In Situ Cell Death Detection Kit (Roche) following the manufacturer's instructions.

Immunoprecipitation and Western blot analysis

For immunoprecipitation cells were lysed in Saito modified buffer (50 mmol/L Tris–HCl, pH 7.4, 0.15 mol/L NaCl, 0.5%

Published OnlineFirst September 10, 2015; DOI: 10.1158/0008-5472.CAN-15-0439

Triton-X100, 5 mmol/L EDTA) containing protease inhibitors mix (Roche). Immunoprecipitations were performed by preclearing lysates with protein G-sepharose (Pierce) and then incubated with the indicated antibody, under gentle rocking at 4°C overnight. For Western blot analysis, cells were lysed in RIPA buffer. SDS-PAGEs were transferred onto PVDF membranes (Millipore). Membranes were developed using the enhanced chemiluminescence (ECL Amersham) by chemiluminescence imaging system, Alliance 2.7 (UVITEC Cambridge) and quantified by the software Alliance V_1607. Primary antibodies: anti-MDM4 BL1258 (Bethyl Laboratory), anti-p53 FL393 (Santa Cruz Biotechnology) and PAb421 (Calbiochem), anti-MDM2 2A10 (kindly provided by M.E. Perry) and Ab1 (Calbiochem), anti-GFP (Roche), anti-FITC (Abcam), anti-BIK/NBK (FL-160; Santa Cruz Biotechnology), anti-phospho-histone H2A.X, anti-PARP-1 (Cell Signaling Technology), anti-α-tubulin DM1A (Sigma), anti-actin C-40 (Sigma).

Isolation of nuclear/cytoplasmic fractions

Nuclear and cytoplasmic fractions were prepared as follows: cells scraped with PBS were resuspended in hypotonic lysis buffer (10 mmol/L HEPES pH 7.9, 10 mmol/L KCl, 0.1 mmol/L EDTA, 0.1 mmol/L EGTA) added with protease inhibitors (Roche). After resuspension, NP-40 was added to a final concentration of 0.6% and the nuclei were pelleted by centrifugation at 10,000 rpm for 30 seconds at 4°C. Supernatant was collected as cytoplasmic fraction. Nuclei pellet was resuspended in nuclear extract buffer (20 mmol/L HEPES pH 7.9, 25% glycerol, 0.4 mol/L NaCl, 0.1 mmol/L EDTA, 0.1 mmol/L EGTA), rocked for 15 minutes at 4°C and then recovered by centrifugation at 14,000 rpm for 5 minutes at 4°C. The pellet containing the chromatin enriched fraction was resuspended in nuclear extract buffer and sonicated by Heat Systems UltraSonics Inc Sonicator W-375 Cell Disruptor at 20% of maximum output power for 30 seconds.

Clonogenicity assay

MCF7 (250 and 500 cells), and MCF10A (5,000 and 10,000 cells) were plated in complete medium in triplicate in 6, 0, and 35 mm dishes, respectively. Treatments (DMSO 0.1%, Pep3 10 μmol/L, Pep3M 10 μmol/L) were administered every 2 days. Dishes were stained by crystal violet.

Nude mice study

CD1-Foxn1^{nu} 6-week-old male mice were injected subcutaneously with luciferase engineered HCT116 (5×10^6/tumor), or GTL-16 (2×10^6/tumor) in Matrigel 10 mg/mL (dilution 1:1; BD Biosciences) to induce tumor formation. After detection of palpable tumor (tumor volume ≥ 70 mm^3), mice were treated with either Pep3 or control Pep3M injected intratumorally at a dose of 10 mg/kg and tumor growth was followed and analyzed by luciferase activity during time. Light emission was detected using the IVIS Lumina II CCD camera system, and the bioluminescent signal was analyzed with the Living Image 2.20 software package (Caliper Life Sciences). All animal experiments were conducted in accordance with institutional guidelines, in the full observation of the Directive 2010/63/UE. GTL-16 cells were infected with lentiviral vector pMA3160 (Addgene) to generate luciferase-expressing cells. HCT116 were transfected with pcDNA-Luc and pBABE Puro and selected using 1 mg/mL puromycin.

RNA extraction and analysis

Total RNA from HCT116 cells untreated or treated with DMSO, Pep3M, or Pep3 was isolated using RNA Purification columns (Norgen, Purification Plus kit) following the manufacturer's instruction. Biologic triplicates were performed. RNA quality was assessed by Bioanalyser (RIN $\geq$ 9.6). After *in vitro* retrotranscription (Applied Biosystem), real-time PCR was performed using ABI 7900 (Applied Biosystem) and SYBR Green Master Mix (Bioline) using the following primers:

(i) BIK (human, BIK, PCR product = 70 bp)fw: 5′-GAATGCATGGAGGGCAGTGAC-3′; rev: 5′-GGCTCACGTCCATCTCGTC-3′

(ii) PIG3 (human, TP53I3, PCR product = 71 bp)fw: 5′-AATGCAGAGACAAGGCCAGT-3′; rev: 5′-GTCCAGATGCCTCAAGTCCC-3′

(iii) GAPDH (human, GAPDH, PCR product = 184 bp)fw: 5′-GAGTCAACGGATTTGGTCGT-3′; rev: 5′-GACAAGCTTCCCGTTCTCAG-3′

(iv) p21 (human, p21, PCR product = 65 bp)fw: 5′-CTGGAGACTCTCAGGGTCGAAA-3′; rev: 5′-GGCGTTTGGAGTGGTAGAAATC-3′

(v) MDM2 (human, MDM2, PCR product = 88 bp)fw: 5′-ATATACCATGATCTACAGGAACTTGGTAGT-3′;rev:5′-GGTGACACCTGTTCTCACTCACA-3′

(vi) TBP (human, TBP, PCR product = 169 bp)fw: 5′-GCACAGGAGCCAAGAG -3′; rev: 5′-GTGGGTGAGCACAAGG-3′. Relative mRNA levels, normalized to TBP, were calculated as follows: $2^{-[\Delta C_t(\text{Pep3 or Pep3M})-\Delta C_t(\text{DMSO})]} = 2^{-\Delta\Delta C_t}$, where ΔC_t equals C_t (BIK, PIG3, GAPDH, p21, or MDM2) $- C_t$ (TBP).

Whole genome expression profiling

The gene expression profiling was performed according to the standard Agilent one-color microarray protocol (Agilent Technologies). The cy3-labeled cRNA was hybridized to Agilent 8 × 60K whole human genome chip. Images were acquired by Agilent Scanner; expression data were extracted by Feature Extraction. Data quality filtering and analysis was performed by GeneSpring GX and Microsoft Excel. Microarray functional data analysis was generated through the IPA webtool (27). Clustering analysis was done using MultiExperiment Viewer. Genes associated to specific cancer features were selected on the basis of the annotations in the Cancer Gene Index of the NCI.

Chromatin immunoprecipitation

HCT116 were untreated or treated with 10 μmol/L Pep3 or Pep3M for 24 hours and then incubated in culture media containing 1% formaldehyde for 10 minutes at room temperature. After formaldehyde neutralization, cells were washed and harvested by ice-cold PBS. Cell lysis was performed in lysis buffer (5 mmol/L PIPES pH 8.0, 85 mmol/L KCl, 0.5% NP-40, protease inhibitors) and nuclei were collected and suspended in nuclei lysis buffer (50 mmol/L Tris-HCl pH 8.0, 10 mmol/L EDTA, 1% SDS, protease inhibitors). Nuclei were sonicated by using a Bioruptor sonicator. Extracts were precleared with protein G (Invitrogen), and 50 μg of DNA were used for immunoprecipitation. An aliquot of precleared lysate was taken as input control. Immunoprecipitation was carried out with anti-p53 sheep polyclonal antibody (Ab-7 Calbiochem), conjugated to paramagnetic protein G beads (Invitrogen). Immune complexes were eluted in elution buffer (50 mmol/L $NaHCO_3$ and 1% SDS) by heating to 65°C for 15 minutes. DNA was purified by using QIAquick PCR

Published OnlineFirst September 10, 2015; DOI: 10.1158/0008-5472.CAN-15-0439

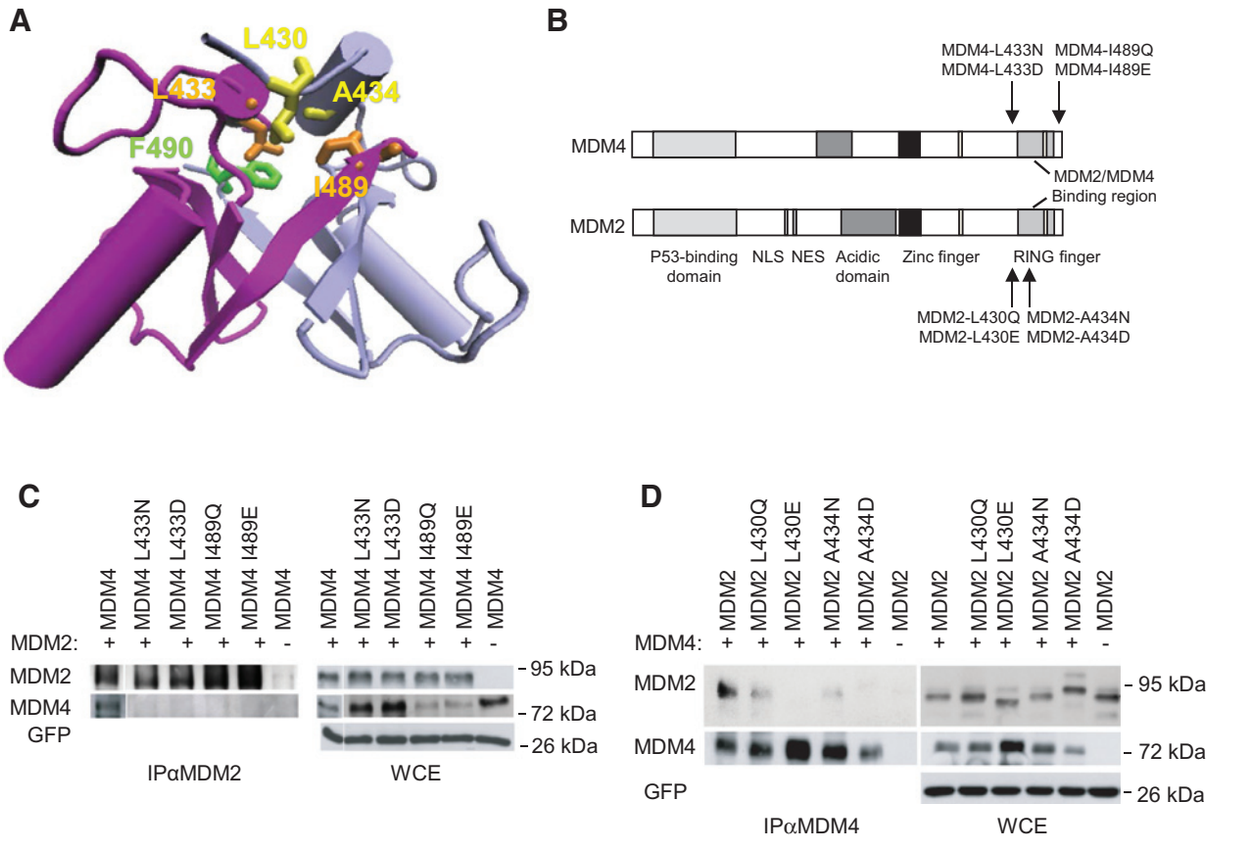

Figure 1.
Characterization of MDM2/MDM4 interaction interface. A, three-dimensional model of the interaction interface of MDM2/MDM4 C-terminal RING finger domains. The purple structure refers to MDM4, the light blue to MDM2. B, schematic drawing of MDM2 and MDM4 proteins with indicated point mutations. C and D, analysis of MDM2 (C) and MDM4 (D) coimmunocomplexes in *p53*$^{-/-}$*Mdm2*$^{-/-}$*Mdm4*$^{-/-}$mouse embryonic fibroblasts (TKO-MEF) transiently expressing the indicated proteins. GFP was used as control of transfection and of loading.

Purification Kit (Qiagen). Purified DNA was analyzed by quantitative real-time PCR using SYBR Green ABI7900. The promoter-specific primer sequences used were as follows: PIG3 5′-GATCCCAGGACTGCGTTTTGCC-3′; 5′-GGGAACGAGACCCAACCTCTTG-3′; MDM2 5′-GCAGGTTGACTCAGCTTTTCCTCT-3′; 5′-GTGGTTACAGCCCCATCAGTAGGTA-3′.

Reactive oxygen species analysis

HCT116 and MCF7 cells were plated in 96-well plates and treated with Pep3, Pep3M, or DMSO. After 48 or 72 hours, cells were washed with PBS and incubated with 25 μmol/L 2′,-7′-dichlorodihydrofluorescein diacetate (H2DCFDA, Sigma) in serum-free media at 37°C for 30 minutes. Cells were then washed once in PBS and incubated for 3 hours in complete media supplemented with or without 100 μmol/L H_2O_2. The fluorescent signal from fluorescent 2′-7′-dichlorodihydrofluorescein (DCF) was monitored by multimode plate reader Enspire (Perkin Elmer). The obtained results were normalized for the number of cells/well by Cell Titer viability assay (Promega).

Results

Characterization of the MDM2–MDM4 interaction interface

MDM2 and MDM4 form heterodimers via association of their C-terminal RING finger domains (28) and the last residues of these domains play a crucial role in this interaction and in the heterodimer activity (24, 25). Analyzing the structural complex of these domains (19), three central β-sheet motifs were observed from each RING domain that are engaged in the formation of a tight β-barrel core at the interface. Particularly, the N-terminal regions of MDM2/MDM4 RING finger domains interact with each other adopting α-helix like structures, while the C-terminal regions contribute to the formation of the β-barrel core through hydrophobic interactions (Fig. 1A). Mutagenesis experiments have previously identified residues of MDM2 RING domain involved in the ubiquitin ligase activity of the complex (24, 29–31). Among these, F490, located at the C-terminus of MDM2, forms a hydrophobic patch at the interface of the complex with residues L433 and I489 of MDM4, and L430 and A434 of MDM2 (Fig. 1A). As hydrophobic patches play key roles in stabilizing protein–protein interactions (32), we investigated the role of L433, I489, L430, and A434 as hot spots of MDM2/MDM4 interaction. MDM2 and MDM4 mutants were generated, by mutating the above residues in either a negatively charged residue or a polar uncharged residue (M2-L430E or M2-L430Q, and M2-A434D or M2-A434N; M4-L433D or M4-L433N and M4-I489E or M4-I489Q, respectively; Fig. 1B).

Expression of these mutants in *p53*$^{-/-}$*Mdm2*$^{-/-}$*Mdm4*$^{-/-}$mouse embryonic fibroblasts (TKO-MEF) and coimmunoprecipitation

Published OnlineFirst September 10, 2015; DOI: 10.1158/0008-5472.CAN-15-0439

of MDM2/MDM4 complex revealed that mutation of both MDM4 residues abolishes its binding to MDM2 confirming that they are essential for the binding of the two proteins (Fig. 1C). Conversely, the association of MDM2 mutants to MDM4 was dependent on the replaced residue, with charged residues (L430E and A434D) and polar uncharged residues (L430Q and A434N) abolishing and reducing the binding to MDM4, respectively (Fig. 1D). Collectively, these observations suggest that the hydrophobic interactions promoted by the side chains of L433 and I489 from MDM4 are important for the stabilization of the RING domain complex. Conversely, MDM2/MDM4 complexes tolerate the replacement of L430 and A434 from MDM2 with polar uncharged residues to some extent, though not standing the presence of charged residues. Noteworthy, the ubiquitinating activity of all mutants but MDM2L430Q, is abolished (Supplementary Fig. S1A), indicating that these residues are important for MDM2/MDM4 heterodimer formation as well as for MDM2 activity. In fact, all these mutants still bind p53, indicating that loss of p53 ubiquitination is due to impairment of MDM2 activity and that the folding of the MDM2 and MDM4 proteins is not affected by the point mutations introduced, at least at the levels of the p53-binding domain (Supplementary Fig. S1B and S1C).

Identification of a peptide that inhibits p53 ubiquitination

From previous data, different peptides that mimic the MDM2 interaction interface of MDM4 were designed. Peptide-3

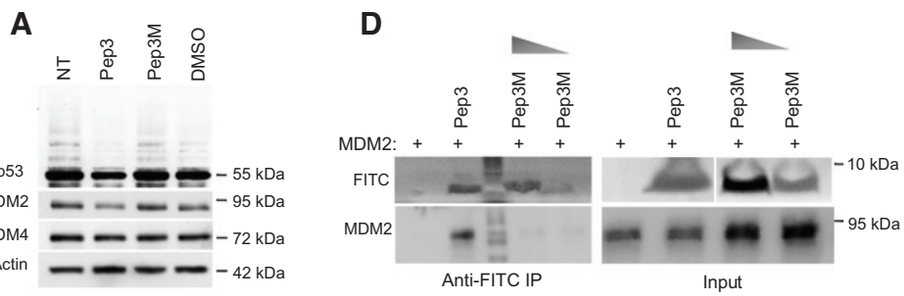

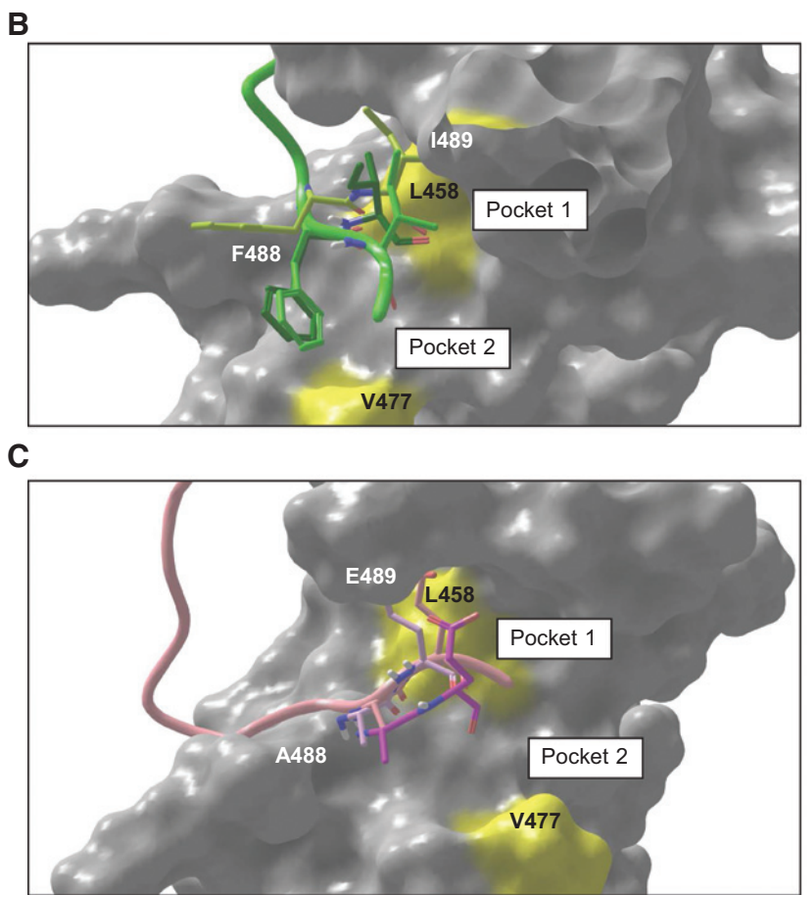

Figure 2.
Peptide-3 features. A, analysis of ubiquitinated forms of p53 in MCF7 cells untreated (NT) or treated with 10 μmol/L Pep3 or Pep3M or solvent (0, 1% DMSO) for 24 hours and for additional 8 hours with 25 μmol/L MG132. B, overlap of three frames of Pep3 at 10 ns (light green sticks), 20 ns (green sticks), and 30 ns (dark green sticks) of the MD trajectory. While I489 stably occupies Pocket 1, F488 undergoes to a conformational change that docks the side chain into Pocket 2. C, overlap of three frames of Pep3M at 10 ns (pink sticks), 20 ns (magenta sticks), and 30 ns (violet sticks) of the MD trajectory. While A488 does not reach Pocket 2, E489 is progressively displaced from Pocket 1 and exposed to the solvent (frame 30 ns, violet sticks). D, Western blot analysis of *in vitro* binding of FITC-Pep3 or FITC-Pep3M to MDM2.

Published OnlineFirst September 10, 2015; DOI: 10.1158/0008-5472.CAN-15-0439

Table 1. Occupancies of stable hydrogen bond interactions (>10%) between the backbone atoms of Pep3 and Pep3M, and MDM2

Pep3				Pep3M			
N	Acceptor (C=O)	Donor (NH)	Occupancy	*N*	Acceptor (C=O)	Donor (NH)	Occupancy
1	Leu430 (MDM2)	Ile481 (Pep3)	12.6%	1	Lys 486 (Pep3M)	Lys 454 (MDM2)	73.7%
2	Ile481 (Pep3)	Leu430 (MDM2)	57.4%	2	Gly456 (MDM2)	Lys486 (Pep3M)	75.2%
3	Ser 428 (MDM2)	Leu483 (Pep3)	58.3%	3	Val487 (Pep3M)	Ser429 (MDM2)	11.7%
4	Leu 483 (Pep3)	Ser428 (MDM2)	41.0%	4	Ala488 (Pep3M)	Gly456 (MDM2)	79.5%
5	Gly456 (MDM2)	Phe488 (Pep3)	83.6%	5	Leu458 (MDM2)	Ala488 (Pep3M)	91.6%
6	Phe488 (Pep3)	Leu458 (MDM2)	85.4%	6	Ala490 (Pep3M)	Leu458 (MDM2)	27.9%
7	Leu458 (MDM2)	Ala490 (Pep3)	15.7%				

(thereafter Pep3), a dodecapeptide that overlaps the COOH-terminus of MDM4 comprising the I489 residue (KEIQLVIKV-FI_{489}A), was able to reduce p53 ubiquitination in different cell lines as compared with untreated or solvent (0,1% DMSO) treated cells (Fig. 2A and Supplementary Fig. S1E). In comparison, a control peptide in which the I489 and the F488 aminoacids were substituted by E489 and A488, respectively (Pep3M, KEIQLVIK-VAEA) did not affect levels of ubiquitinated p53 (Fig. 2A and Supplementary Fig. S1D and S1E). A peptide containing only substitution of I489 retained partial inhibitory activity towards MDM2 (Supplementary Fig. S1E).

Starting from the structural data of MDM2/MDM4 RING domains, MD simulations of Pep3 and Pep3M in complex with the MDM2-RING domain were used to investigate the molecular basis of their binding modes to MDM2. Pep3 is stably anchored to MDM2, with the backbone oxygen and nitrogen atoms engaged in a pattern of stable hydrogen bonds with the backbone atoms of MDM2 (Table 1). The side chain of MDM4-I489 stably occupies a hydrophobic pocket defined by residue L458 of MDM2 (Pocket 1, Fig. 2B) along the entire MD trajectory. MDM4-F488 undergoes a conformational change docking its side chain into a second hydrophobic pocket (Pocket 2, Fig. 2B) defined by residue V477 of MDM2. Although Pep3M makes six stable backbone-mediated hydrogen bonds with MDM2 (Table 1), it does not occupy the two hydrophobic pockets (Fig. 2C). Specifically, the side chain of A488 is too short to reach Pocket 2, and the polar side chain of E489 is not suited to occupy the hydrophobic Pocket 1. These data provide a likely explanation as for why Pep3, but not Pep3M, binds to MDM2, with the former peptide matching two hydrophobic patches (Pocket 1 and 2) at the interface of the complex. These data highlight also the role of MDM4-F488 in the interaction of MDM4/Pep3 to MDM2 and explain the partial activity of the peptide-3 mutated in the I489 only. *In vitro* binding assays confirmed Pep3/MDM2 interaction. Pep3 conjugated to the fluorescein-isothiocyanate group (FITC-Pep3) was indeed able to coimmunoprecipitate MDM2, whereas increasing doses of FITC-Pep3M did not (Fig. 2D).

Pep3 induces p53-dependent cancer cell death

We next tested the cell-penetrating activity of FITC-Pep3 *in vivo*. Strikingly, internalization of the peptide in a time and dose-dependent manner was observed upon its addition to the culture medium of the human cancer cell line MCF7 (Fig. 3A and B). Confocal imaging showed an intense FITC-Pep3 staining confined to vesicular structures frequently surrounding the nucleus. In addition, several FITC-Pep3–positive vesicles were observed in proximity to the plasma membrane indicative of an active internalization process of FITC-Pep3. Similar results were obtained for Pep3M (Supplementary Fig. S2A). FACS analysis allowed us to quantify the high proportion of FITC-positive cells (Fig. 3B and Supplementary Fig. S2B). Similar results were obtained with the colorectal cancer cell line HCT116. Interestingly, the FITC-Pep3–positive HCT116 cells showed a significant increase of apoptotic cell death compared with FITC-Pep3M–treated cells (Fig. 3C and Supplementary Fig. S2C). In contrast, Pep3 and Pep3M peptides caused only a limited increase of cell death in HCT116 cells lacking functional p53 ($p53^{-/-}$HCT116), indicating that Pep3-induced apoptosis is dependent on the presence of p53 (Fig. 3C). Similar results were obtained when using untagged peptides (Supplementary Fig. S2D). In contrast, scramble peptides (SC3A and SC3B) containing the same aminoacids present in Pep3 but assembled in a different order did not induce cell death (Supplementary Fig. S2E), confirming the specificity of Pep3 activity.

Treatment of HCT116 cells with increasing doses of Pep3 (2, 5, 10, 20, 30 μmol/L) showed dose-dependent cell death reaching a plateau at 20 μmol/L (Fig. 3D). Pep3 also induced apoptosis in wt-p53 GTL-16, MCF7 (Fig. 3E), and HEPG2 (Supplementary Fig. S2F) cell lines. Conversely, it was ineffective in p53-null H1299 (Supplementary Fig. S2G) or in p53-knockdown MCF7 cells (shp53-MCF7) (Fig. 3F). Importantly, Pep3 did not significantly increase cell death in MDM2-knockdown GTL-16 cells (siMDM2-GTL-16), indicating that its activity requires the presence of MDM2 (Fig. 3G and Supplementary Fig. S2H). Pep3 also significantly inhibited colony formation in MCF7 cells in comparison with control cells, suggesting its ability to affect the tumorigenic potential of cancer cells *in vitro* (Fig. 3H). Importantly, Pep3 did not increase apoptotic cell death nor affected cell-cycle profile or colony forming ability in untransformed MCF10A cells (Fig. 3I and J and Supplementary Fig. S3A). Similarly, it did not increase cell death (by FACS and PARP-1 cleavage analysis) nor affected cell-cycle profile in primary human fibroblasts (Supplementary Fig. S3B–S3D), suggesting that this peptide selectively affects the viability of tumor cells but not of untransformed ones.

Pep3 impairs tumor growth *in vivo*

To assess the therapeutic potential of Pep3 *in vivo*, we tested the antitumor effects of Pep3 in xenograft models. CD1-Foxn1^{nu} mice were injected in both flanks with HCT116, or GTL-16 cells expressing a stable luciferase reporter gene. Once luciferase-positive tumor masses were clearly detected (corresponding to tumor volume $\geq$ 70 mm^3), the mice were randomly divided into two groups and Pep3 or Pep3M injected (10 mg/kg) every other day in one of the two flanks for at least 15 days. Tumor growth was monitored by measuring bioluminescence and quantified as percentage of the bioluminescence of the treated versus untreated contralateral tumor. Whereas Pep3 significantly reduced tumor growth, Pep3M had only a marginal effect (Fig. 3K and L and Supplementary Fig. S4A). The p53 protein showed comparable levels in all samples, suggesting that the gene remained wild-type

Published OnlineFirst September 10, 2015; DOI: 10.1158/0008-5472.CAN-15-0439

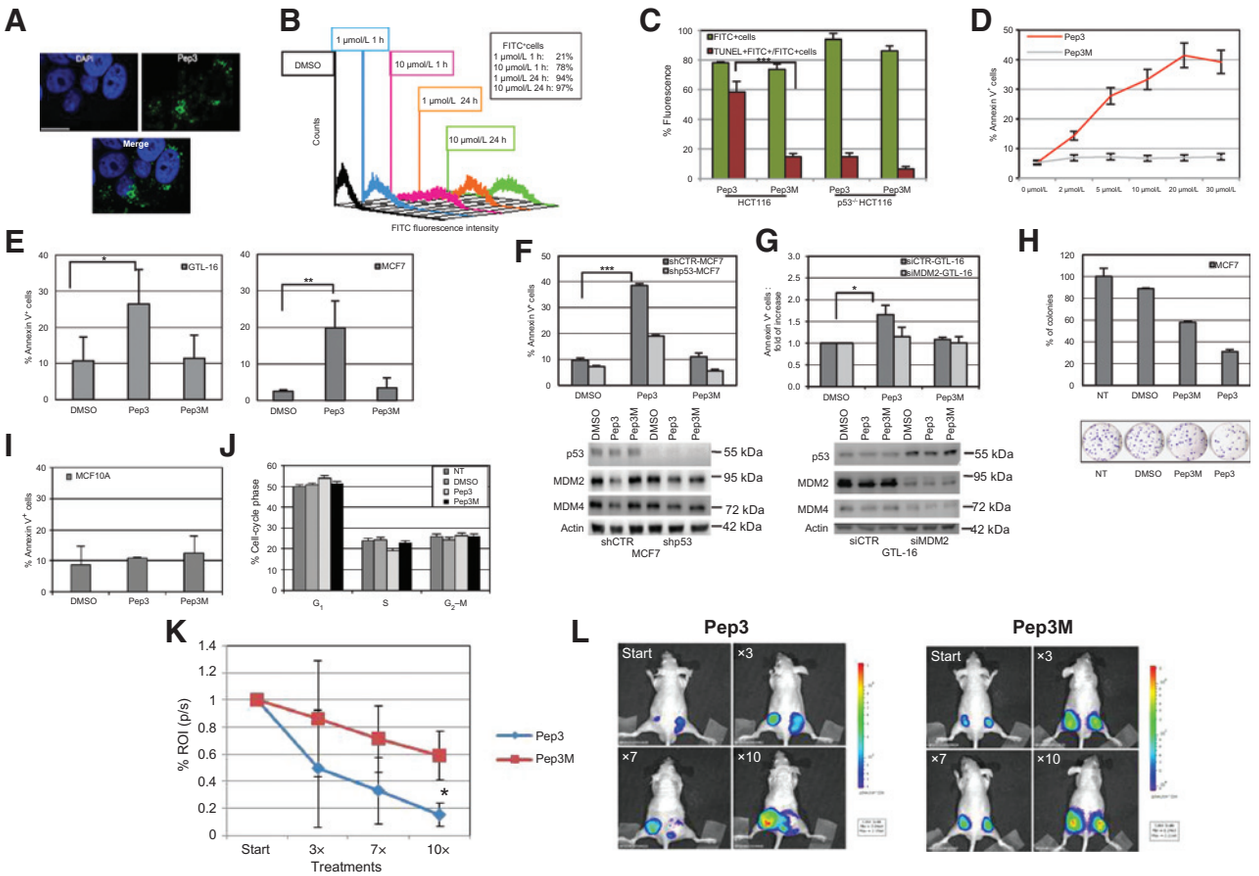

Figure 3.

In vitro and *in vivo* biologic activity of Pep3. A, confocal optical planes from a z-stack acquisition showing 1 μmol/L FITC-Pep3 intracellular localization after 24 hours treatment. Scale bar, 15 μm. B, FACS analysis of MCF7 cells treated with Pep3 as indicated. C, percentage of $FITC^+$ and double $TUNEL^+FITC^+/FITC^+$ $p53^{+/+}$ HCT116 (HCT116) or $p53^{-/-}$ HCT116 cells treated with indicated peptides for 24 hours ($N \geq 3$; ***, $P < 0.001$; **, $P < 0.01$; *, $P < 0.05$, Student *t* test). D, cell death by Annexin V staining of HCT116 treated with Pep3 (red line) or Pep3M (black line) for 48 hours. E, cell death by Annexin V staining following DMSO, Pep3, or Pep3M treatment for 48 hours in GTL-16 (left) and for 72 hours in MCF7 (right). Mean ± SD of at least three different experiments is shown. F, cell death by Annexin V staining of pSuper.retro-iscrambleMCF7 (shCTR-MCF7) or pSuper.retro-ip53MCF7 cells (shp53-MCF7) following indicated treatments (top). Mean ± SD of at least three different experiments is shown. Western blot analysis of indicated proteins from a representative experiment performed as in the top (bottom). G, cell death by Annexin V staining of GTL-16 cells transfected with 30 nmol/L stealth control siRNA (siCTR-GTL-16) or stealth siMDM2-RNA (siMDM2-GTL-16) and after 24 hours exposed to the indicated treatments for 24 hours (top). Annexin V positivity of DMSO-treated cells was set to 1. Mean ± SD of at least three different experiments is shown. Western blot analysis of indicated proteins from a representative experiment as in the top (bottom). H, clonogenic assay using MCF7 treated as indicated. Bottom, representative of an experiment performed in triplicate. I, cell death by Annexin V staining following DMSO, Pep3, or Pep3M treatment for 48 hours in MCF10A. J, FACS analysis of cell-cycle phases of MCF10A treated as indicated. Mean ± SD of three different experiments is shown. K, quantification of emitted light from tumor xenografts. A total of 5×10^6 HCT116 were injected subcutaneously and after 10 days treated with 10 mg/kg Pep3 or Pep3M every other day. Bioluminescence was detected at days 0 (start), 6 (3×), 14 (7×), and 20 (10×) of treatment. Mean ± SD is shown. Photon emission is measured as photons per second (p/s). ($N \geq 6$; *, $P < 0.05$, Student *t* test). L, bioluminescence of a representative mouse at different life times after treatment of the tumor in the right flank with Pep3 (left) or Pep3M (right) on days 0, 6, 14, and 20. Light emitted from the animals appears in pseudocolor scaling.

during the course of the experiment (see Fig. 4C). No significant host toxicity was observed as evaluated by animal weight (Supplementary Fig. S4B). Accordingly, FITC-Pep3 injection in the hind limb muscle of mice showed no diffusion of the fluorescence signal within 24 hours (Supplementay Fig. S4C). Taken together, these data demonstrate that Pep3 effectively suppresses tumor growth *in vivo*, and confirm that the MDM4/MDM2 interaction interface is a potential molecular target for anticancer therapy.

Pep-3 increases levels of p53 bound to chromatin

To understand Pep3 activity, we analyzed the effects of Pep3 treatment at the molecular level. Pep3 exposure caused a marked decrease of full-length PARP-1 (fl-PARP-1), a marker of cell apoptosis, in both MCF7 and HCT116 cells (Fig. 4A and B). Caspase-3 cleavage was not detected, suggesting the involvement of caspase-7 in PARP-1 cleavage (33). Importantly, fl-PARP-1 was significantly decreased also in Pep3-treated but not in Pep3M-treated xenograft tumor samples (Fig. 4C and D), indicating that Pep3-induced suppression of tumor growth is likely caused by *in vivo* cell apoptosis. Unexpectedly, Pep3-induced apoptosis did not correlate with an increase in p53 steady-state protein levels (Fig. 4A–C). However, analysis of p53 subcellular distribution revealed a significant Pep3-mediated increase in the pool of p53 bound to chromatin at the detriment of its soluble/nucleoplasmic

Published OnlineFirst September 10, 2015; DOI: 10.1158/0008-5472.CAN-15-0439

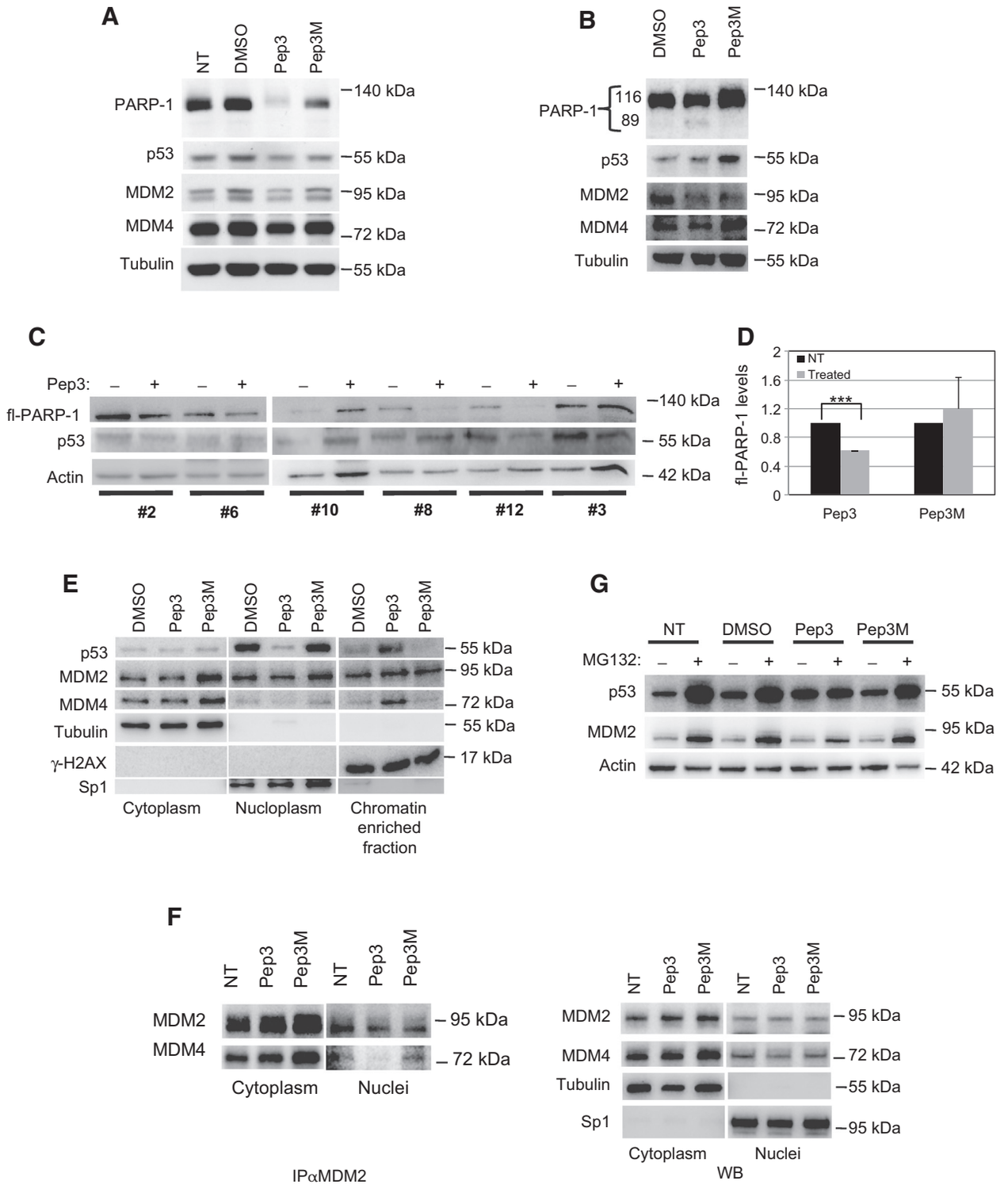

Figure 4.
Molecular activities of Pep3. A and B, Western blot analysis of indicated proteins in MCF7 cells (A) and HCT116 (B) treated as indicated for 72 (A) or 24 hours (B). C, Western blot analysis of indicated proteins in HCT116 tumor xenograft samples untreated or treated with Pep3. Numbers under the blot refer to the mouse number identification. D, quantification of fl-PARP-1 levels in xenograft samples. Each sample was normalized to the tubulin and quantified as percentage to the fl-PARP-1 levels in the contralateral tumor. Bars, mean ± SD of Pep3- and Pep3M-treated tumors. ($N \geq 6$; ***, $P < 0.001$, Student t test). E, Western blot analysis of indicated proteins in subcellular fractions of MCF7 cells treated as indicated for 24 hours. G, Western blot analysis of indicated proteins in MCF7 cells treated as indicated for 24 hours and for additional 8 hours with 25 μmol/L MG132. F, immunoprecipitation (left) and Western blot analysis (right) of MCF7 cells treated as in A. MDM2 was immunoprecipitated using 2A10/Ab1 mix.

Published OnlineFirst September 10, 2015; DOI: 10.1158/0008-5472.CAN-15-0439

fraction (Fig. 4E). The MDM4 protein was redistributed similarly to p53, whereas MDM2 subcellular distribution was not affected by Pep3 (Fig. 4E). These data are consistent with an alteration of the MDM2/MDM4 nuclear complexes upon Pep3 addition. In fact, association between MDM4 and MDM2 was reduced by Pep3 in the nuclear fraction but not in cytoplasmic extract (Fig. 4F and Supplementary Fig. S5A). Treatment with the proteasome inhibitor MG132 did not exacerbate the Pep3-dependent increase in p53 protein levels, including the chromatin bound fraction (Fig. 4G), confirming that Pep3 interferes with p53 degradation.

The levels of phosphorylated histone H2AX (γ-H2AX), a marker of DNA damage did not increase upon Pep3 exposure (Fig. 4E), indicating that recruitment of p53 to the chromatin is not associated with activation of the DNA damage response. Accordingly, phosphorylation of p53 at Ser46 or Ser15, two features of stress-mediated p53 activation were not observed (Supplementary Fig. S5B and S5C).

Pep3 induces p53-dependent transcriptional activation of proapoptotic/oxidant targets

Transcriptionally active p53 can induce apoptosis through different target genes (34). Genome-wide transcriptomic analysis of Pep3-treated HCT116 cells compared with untreated, DMSO or Pep3M-treated cells, identified 347 and 198 genes that were significantly deregulated 24 and 48 hours after treatment respectively (Supplementary Tables S1 and S2). Overlapping of the two groups of genes deregulated at 24 and 48 hours revealed a significant alteration of a common subgroup of 49 genes (Fig. 5A and Supplementary Fig. S6). Clusters corresponding to the different treatments were clearly apparent on a principal component analysis (PCA; Fig. 5B).

Ingenuity Pathways Analysis revealed that most of the 347 mRNAs deregulated by Pep3 encode for proteins involved in cell death and survival (Fig. 5C and Supplementary Fig. S6E). Of note, p53 was identified as one of the top putative upstream regulators of these genes confirming that Pep3 induces p53 activity (Fig. 5D).

Among the well-established p53 target genes induced by Pep3 are two genes encoding for proapoptotic and pro-oxidant factors: BCL2 interacting killer, *BIK/BP4/NBK/BIP1* (35), and tumor protein p53-inducible protein-3, *PIG3/TP53I3* (Fig. 5D; ref. 36). qRT-PCR confirmed the significant induction of these mRNAs at 24 (Fig. 5E) and 48 hours (Supplementary Fig. S6F), whereas, in comparison, *p21/WAF1* and *MDM2*, two p53 target genes, involved mainly in growth arrest, were not induced by Pep3. Chromatin immunoprecipitation (ChIP) confirmed the increased recruitment of p53 at the promoter of *PIG3* in cells exposed to Pep3 (Fig. 5F). In contrast, no increased recruitment of p53 at the *MDM2* promoter in the same experimental conditions was observed (Supplementary Fig. S7A). Consistent with these findings, BIK protein levels were highly increased upon Pep3 exposure both in MCF7 and HCT116 cells (Fig. 6A and B and Supplementary Fig. S7B). Of importance, siBIK by single oligos or their mix (Supplementary Fig. S8A) resulted in decreased PARP-1 cleavage (Fig. 6B) and Pep3-induced cell apoptosis (Supplementary Fig. S9A), confirming the role played by this gene in Pep3-mediated activity. Given the involvement of BIK and PIG3 in p53-mediated oxidative stress response (36, 37), we quantified reactive oxygen species (ROS) levels using the fluorogenic probe DCF upon H_2O_2 stimulation. This analysis revealed a significant increase of intracellular ROS levels following Pep3 exposure both in HCT116 and MCF7 cells (Fig. 6C and Supplementary Fig. S9B), confirming that Pep3 counteracts the antioxidant potential of the cell. The Pep3-dependent increase of ROS levels in HCT116 cells was detectable even in the absence of H_2O_2 stimulation (Fig. 6C). Importantly, ROS levels were not induced by Pep3 in $p53^{-/-}$HCT116 cells (Fig. 6C), confirming the crucial role played by p53 in this Pep3-induced response. Finally, siBIK or siPIG3 (Supplementary Fig. S8) rescued the increase of ROS levels mediated by Pep3 treatment (Fig. 6D), confirming the role played by these genes in this response.

Discussion

Most of the pharmacologic approaches aiming at reactivating p53 in cancer cells have focused to date on the interaction interface between p53 and MDM2 or MDM4. Here, we developed an alternative strategy that aims at inhibiting the activity of the MDM2/MDM4 complexes by interfering with their heterodimerization. Our study demonstrates that the binding of a peptide mimicking the MDM4 C-terminus tail to MDM2, impairs MDM2-mediated p53 ubiquitination and activates p53-dependent transcription and oncosuppressive activities.

Interestingly, our data indicate that Pep3 may be mainly effective towards a specific subcellular pool of MDM2/MDM4/p53 as evidenced by the alteration of the nuclear complexes but not of the cytoplasmic fraction. Consistently, the p53 transcriptional program activated by Pep3 is restricted to some p53 target genes involved in the oxidative stress response, suggesting a specific control of this function by the MDM2/MDM4 complexes. In fact, MDM2 and MDM4 act as cotranscriptional inhibitors at the p53-responsive elements on the promoter of *PIG3*, but not of *MDM2* or *RCHY1/PIRH2* genes (21). In addition, MDM2 mediates histone ubiquitylation and transcriptional repression (38). At present, it is not known whether subcellular MDM2/MDM4 complexes present different features. The conformation assumed by the complexes consequent to DNA binding might contribute to the selective sensitivity of the nuclear heterodimers to Pep3. Alternatively, additional partners and/or post-translational modifications may distinguish the subcellular complexes.

In contrast to the majority of the approaches that target the interaction between p53 and MDM2, our method causes p53-dependent cell death of various cancer cells, supporting the requirement of the heterodimer for efficient control of p53 function. The observation that the preferred response elicited by Pep3 is apoptosis is also in agreement with recent data from our and other labs that reported impairment of MDM4/MDM2 heterodimer function during apoptosis (22, 39–41). Importantly, this observation highlights the potential therapeutic value of targeting the MDM2/MDM4 heterodimers.

Cancer cells are subjected to increased and persistent oxidative stress and accumulating evidence indicates that increasing ROS levels represents an effective approach to induce cancer cell–specific apoptosis (42–44). Accordingly, the p53-reactivating molecule RITA appears to function by ROS-activating mechanism as Pep3 (45). Our data, indicating that Pep3 reduces the antioxidative potential of the cell and enhances ROS levels, further support the targeting of MDM2/MDM4 complexes as a cancer cell–specific efficient therapeutic strategy. The absence of Pep3 activity in untransformed cell line MCF10A and in human fibroblasts is consistent with this hypothesis.

Compared with the current p53-reactivating approaches, the ability of Pep3 to activate the chromatin-enriched fraction of p53

Published OnlineFirst September 10, 2015; DOI: 10.1158/0008-5472.CAN-15-0439

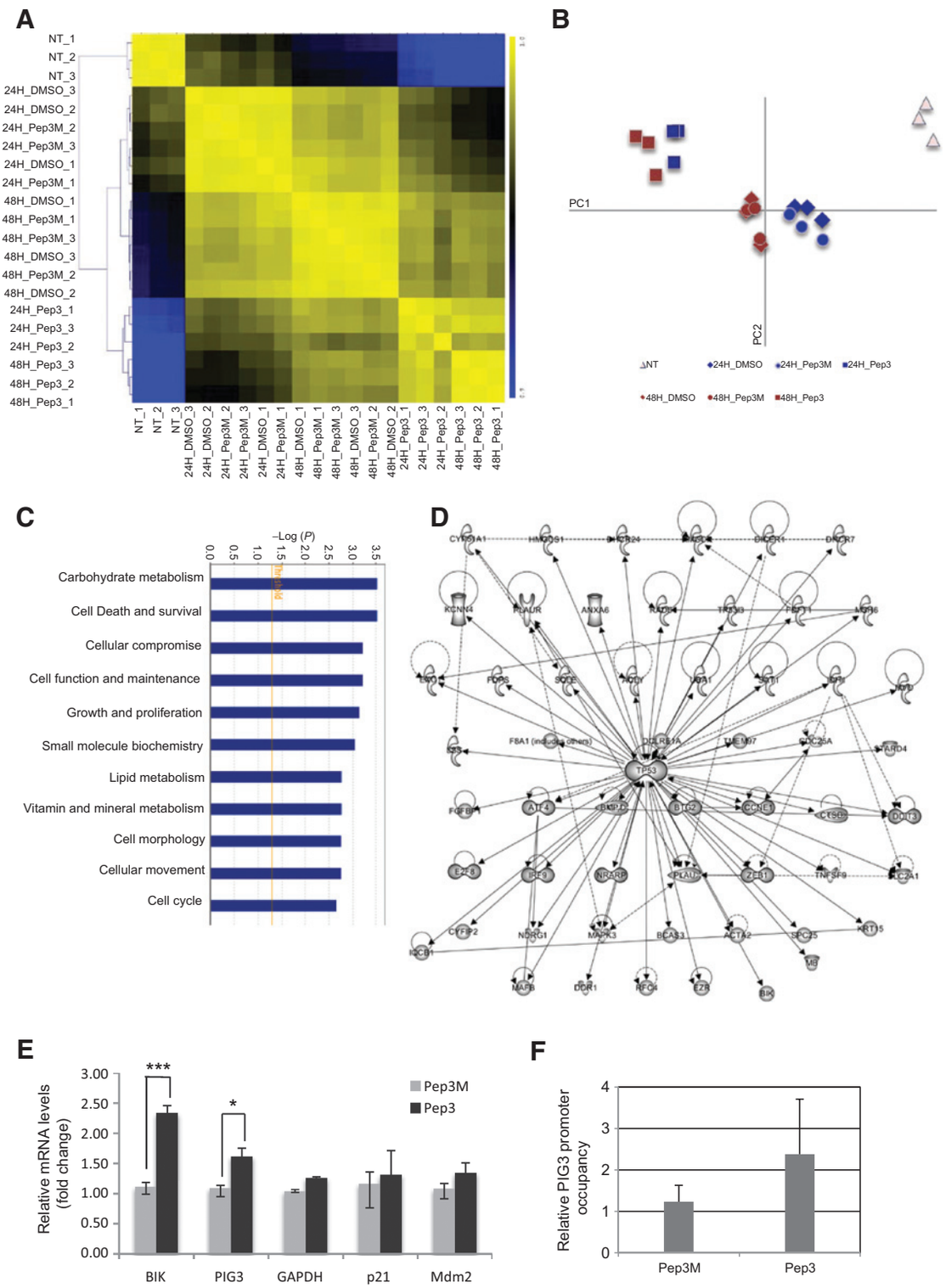

Figure 5.
Transcriptomic analysis of Pep3. A, HCT116 cells were subjected to microarray analysis as untreated (NT) or after DMSO, Pep3M, or Pep3 treatment for 24 or 48 hours (H). Data of three biologic replicates are shown. Pearson correlation coefficient of the 49 genes significantly differentially expressed between Pep3 and Pep3M at both 24 and 48 hours is shown. B, PCA analysis of samples as in A. C, biofunctional analysis of the 356 genes differentially expressed in HCT116 cells after 24 hours Pep3 treatment. D, network of p53 downstream genes differentially expressed after 24 hours Pep3 treatment. E, mRNA levels by qRT-PCR of *BIK, PIG3, GAPDH, P21*, and *MDM2* in HCT116 cells treated with Pep3 or Pep3M for 24 hours ($N = 3$; ***, $P < 0.001$; *, $P < 0.05$, Student t test). F, ChIP of p53 on the promoter of *PIG3* gene. Bars, mean ± SD of biologic triplicates.

Published OnlineFirst September 10, 2015; DOI: 10.1158/0008-5472.CAN-15-0439

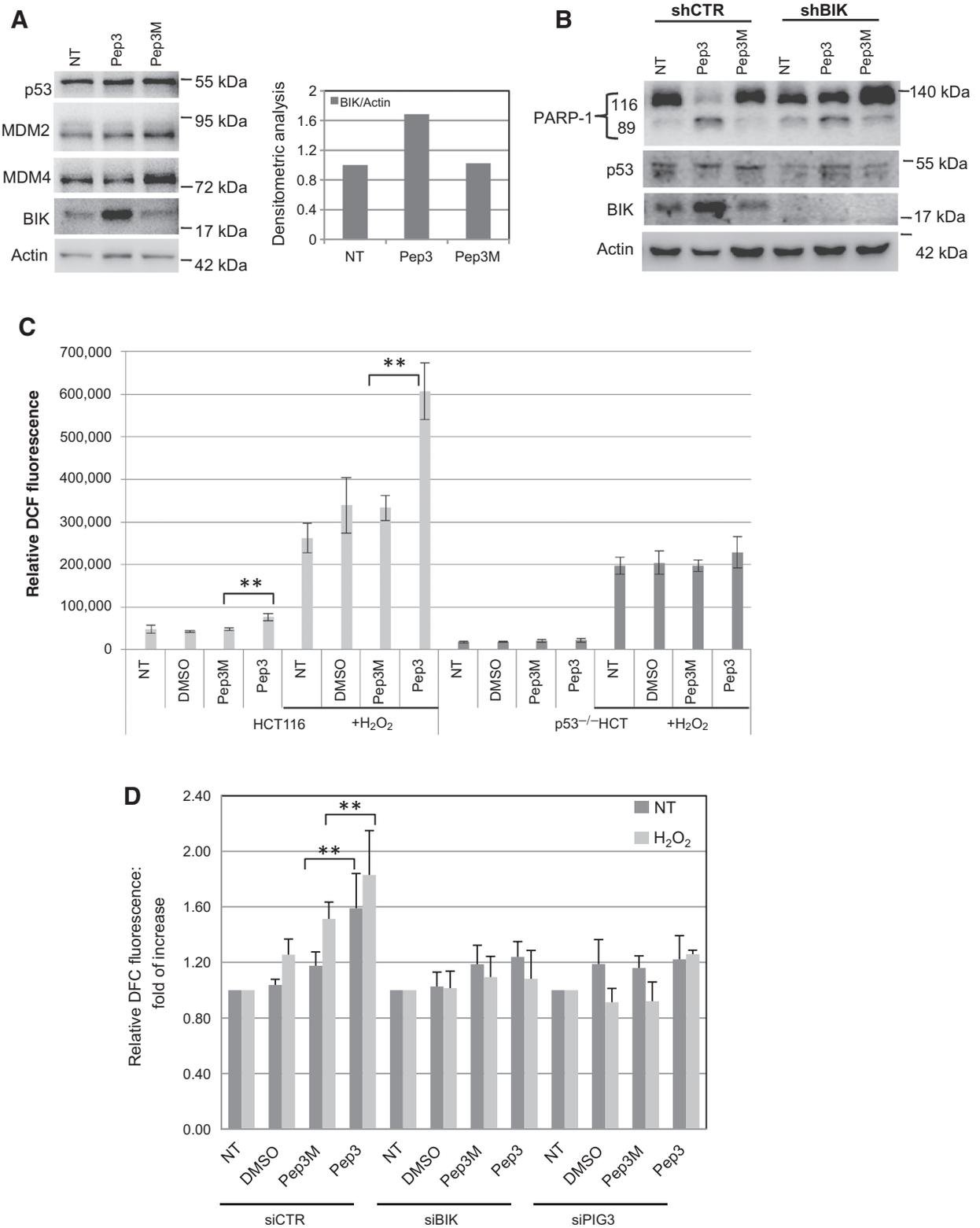

Figure 6.
Effect of Pep3 on oxidative stress. A, Western blot analysis of indicated proteins in MCF7 cells treated as specified (left). Densitometric analysis of BIK protein normalized to the actin levels (right). B, Western blot analysis of indicated proteins in HCT116 transfected with 20 nmol/L stealth control siRNA (siCTR) or stealth BIK siRNA (siBIK mix) for 18 hours and then treated as indicated for 48 hours. C, analysis of ROS accumulation in untreated (NT), DMSO, Pep3M-, or Pep3-treated HCT116 and $p53^{-/-}$HCT116 cells for 48 hours without or with 100 μmol/L H_2O_2. Bars, mean ± SD of relative DCF fluorescence intensity normalized to cell viability (by CellTiter Blue assay) of biologic triplicates performed in quadruplicates ($N = 3$; **, $P < 0.01$, Student t test). D, analysis of ROS as in C using HCT116 transfected with 20 nmol/L stealth siRNA (siCTR, siBIK, siPIG3) for 24 hours and then treated as indicated for additional 48 hours.

Published OnlineFirst September 10, 2015; DOI: 10.1158/0008-5472.CAN-15-0439

might endow this strategy of reduced toxicity. In fact, in a recent exploratory clinical trial, the p53-activating molecule RG7112, a member of Nutlin family, has shown treatment-related serious adverse events (46), all of which related to haematologic toxicity (47) caused probably by the treatment-derived high levels of p53. Similarly, highly levels of p53 have been observed following the treatment with the unique double MDM2/MDM4 inhibitor developed so far (17).

In addition, given the increased specificity of anticancer peptides in the recognition of their targets (48), Pep3 may overcome side effects and toxicities of other cancer therapies. In fact, small-molecule inhibitors of MDM2-mediated ubiquitinating activity, have shown unintended activities towards other RING finger E3 ligases (49, 50).

On the basis of these data, targeting the MDM2/MDM4 interaction interface appears a promising therapeutic strategy for developing new anticancer lead compounds with high specificity and effectiveness.

Disclosure of Potential Conflicts of Interest

No potential conflicts of interest were disclosed.

Authors' Contributions

Conception and design: M. Pellegrino, A. Macchiarulo, F. Moretti
Development of methodology: M. Pellegrino, F. Mancini, R. Lucà, N. Giacchè, I. Manni, E. Teveroni, M. Buttarelli, L. Fici, T. Bruno
Acquisition of data (provided animals, acquired and managed patients, provided facilities, etc.): F. Florenzano, R. Brandi, M. Fanciulli, M. D'Onofrio, G. Piaggio, R. Pellicciari
Analysis and interpretation of data (e.g., statistical analysis, biostatistics, computational analysis): M. Pellegrino, R. Lucà, A. Coletti, I. Arisi, F. Florenzano, M. Buttarelli, J.C. Marine, A. Macchiarulo, F. Moretti
Writing, review, and/or revision of the manuscript: M. Pellegrino, R. Lucà, A. Pontecorvi, J.C. Marine, A. Macchiarulo, F. Moretti
Administrative, technical, or material support (i.e., reporting or organizing data, constructing databases): M. Pellegrino, R. Lucà
Study supervision: F. Moretti

Acknowledgments

The authors thank Dr. F. Maina for GTL-16 cells, Dr. Cinzia Rinaldo for the pSuper.retro-ip53 plasmid, and Ada Sacchi for her support.

Grant Support

This work was supported by grants from Associazione Italiana Ricerca sul Cancro (AIRC; IG-8825, IG-12767; F. Moretti), Project "FaReBio di Qualita" from Italian Ministry of Economy and Finance to the CNR, FIRB RBAP1153LS_007 (A. Pontecorvi), and FIRB B81J10001870008_RBAP10L8TY_003-MD, FP7 European-Grant PAINCAGE, grant: 603191 (M. D'Onofrio).

The costs of publication of this article were defrayed in part by the payment of page charges. This article must therefore be hereby marked *advertisement* in accordance with 18 U.S.C. Section 1734 solely to indicate this fact.

Received February 16, 2015; revised July 10, 2015; accepted July 14, 2015; published OnlineFirst September 10, 2015.

References

1. Selivanova G. Wild type p53 reactivation: from lab bench to clinic. FEBS Lett 2014;588:2628–38.
2. Khoo KH, Verma CS, Lane DP. Drugging the p53 pathway: understanding the route to clinical efficacy. Nat Rev Drug Discov 2014;13:217–36.
3. Montes de Oca Luna R, Wagner DS, Lozano G. Rescue of early embryonic lethality in mdm2-deficient mice by deletion of p53. Nature 1995;378:203–6.
4. Momand J, Zambetti GP, Olson DC, George D, Levine AJ. The mdm-2 oncogene product forms a complex with the p53 protein and inhibits p53-mediated transactivation. Cell 1992;69:1237–45.
5. Vassilev LT, Vu BT, Graves B, Carvajal D, Podlaski F, Filipovic Z, et al. *In vivo* activation of the p53 pathway by small-molecule antagonists of MDM2. Science 2004;303:844–8.
6. Gudkov AV. Cancer drug discovery: the wisdom of imprecision. Nat Med 2004;10:1298–9.
7. Issaeva N, Bozko P, Enge M, Protopopova M, Verhoef LG, Masucci M, et al. Small molecule RITA binds to p53, blocks p53-HDM-2 interaction and activates p53 function in tumors. Nat Med 2004;10:1321–8.
8. Tovar C, Rosinski J, Filipovic Z, Higgins B, Kolinsky K, Hilton H, et al. Small-molecule MDM2 antagonists reveal aberrant p53 signaling in cancer: implications for therapy. Proc Natl Acad Sci U S A 2006;103:1888–93.
9. Shvarts A, Steegenga WT, Riteco N, van Laar T, Dekker P, Bazuine M, et al. MDMX: a novel p53-binding protein with some functional properties of MDM2. EMBO J 1996;15:5349–57.
10. Patton JT, Mayo LD, Singhi AD, Gudkov AV, Stark GR, Jackson MW. Levels of HdmX expression dictate the sensitivity of normal and transformed cells to Nutlin-3. Cancer Res 2006;66:3169–76.
11. Wade M, Wong ET, Tang M, Stommel JM, Wahl GM. Hdmx modulates the outcome of p53 activation in human tumor cells. J Biol Chem 2006;281:33036–44.
12. Gembarska A, Luciani F, Fedele C, Russell EA, Dewaele M, Villar S, et al. MDM4 is a key therapeutic target in cutaneous melanoma. Nat Med 2012;18:1239–47.
13. Popowicz GM, Czarna A, Holak TA. Structure of the human Mdmx protein bound to the p53 tumor suppressor transactivation domain. Cell Cycle 2008;7:2441–3.
14. Macchiarulo A, Giacche N, Carotti A, Baroni M, Cruciani G, Pellicciari R. Targeting the conformational transitions of MDM2 and MDMX: insights into dissimilarities and similarities of p53 recognition. J Chem Inf Model 2008;48:1999–2009.
15. Joseph TL, Madhumalar A, Brown CJ, Lane DP, Verma CS. Differential binding of p53 and nutlin to MDM2 and MDMX: computational studies. Cell Cycle 2010;9:1167–81.
16. Marine JC, Francoz S, Maetens M, Wahl G, Toledo F, Lozano G. Keeping p53 in check: essential and synergistic functions of Mdm2 and Mdm4. Cell Death Differ 2006;13:927–34.
17. Chang YS, Graves B, Guerlavais V, Tovar C, Packman K, To KH, et al. Stapled alpha-helical peptide drug development: a potent dual inhibitor of MDM2 and MDMX for p53-dependent cancer therapy. Proc Natl Acad Sci U S A 2013;110:E3445–54.
18. Kawai H, Lopez-Pajares V, Kim MM, Wiederschain D, Yuan ZM. RING domain-mediated interaction is a requirement for MDM2's E3 ligase activity. Cancer Res 2007;67:6026–30.
19. Linke K, Mace PD, Smith CA, Vaux DL, Silke J, Day CL. Structure of the MDM2/MDMX RING domain heterodimer reveals dimerization is required for their ubiquitylation in trans. Cell Death Differ 2008;15:841–8.
20. Tollini LA, Jin A, Park J, Zhang Y. Regulation of p53 by Mdm2 E3 ligase function is dispensable in embryogenesis and development, but essential in response to DNA damage. Cancer Cell 2014;26:235–47.
21. Tang Y, Zhao W, Chen Y, Zhao Y, Gu W. Acetylation is indispensable for p53 activation. Cell 2008;133:612–26.
22. Pant V, Xiong S, Iwakuma T, Quintas-Cardama A, Lozano G. Heterodimerization of Mdm2 and Mdm4 is critical for regulating p53 activity during embryogenesis but dispensable for p53 and Mdm2 stability. Proc Natl Acad Sci U S A 2011;108:11995–2000.
23. Huang L, Yan Z, Liao X, Li Y, Yang J, Wang ZG, et al. The p53 inhibitors MDM2/MDMX complex is required for control of p53 activity *in vivo*. Proc Natl Acad Sci U S A 2011;108:12001–6.
24. Poyurovsky MV, Priest C, Kentsis A, Borden KL, Pan ZQ, Pavletich N, et al. The Mdm2 RING domain C-terminus is required for supramolecular assembly and ubiquitin ligase activity. EMBO J 2007;26:90–101.

Published OnlineFirst September 10, 2015; DOI: 10.1158/0008-5472.CAN-15-0439

25. Uldrijan S, Pannekoek WJ, Vousden KH. An essential function of the extreme C-terminus of MDM2 can be provided by MDMX. EMBO J 2007; 26:102–12.
26. Kräutler V, van Gunsteren WF, Hünenberger PH. A fast SHAKE algorithm to solve distance constraint equations for small molecules in molecular dynamics simulations. J Comput Chem 2001;22:501–08.
27. 2015 Home - Ingenuity. <http://www.ingenuity.com/>.
28. Tanimura S, Ohtsuka S, Mitsui K, Shirouzu K, Yoshimura A, Ohtsubo M. MDM2 interacts with MDMX through their RING finger domains. FEBS Lett 1999;447:5–9.
29. Singh RK, Iyappan S, Scheffner M. Hetero-oligomerization with MdmX rescues the ubiquitin/Nedd8 ligase activity of RING finger mutants of Mdm2. J Biol Chem 2007;282:10901–7.
30. Wade M, Li YC, Matani AS, Braun SM, Milanesi F, Rodewald LW, et al. Functional analysis and consequences of Mdm2 E3 ligase inhibition in human tumor cells. Oncogene 2012;31:4789–97.
31. Egorova O, Sheng Y. A site-directed mutagenesis study of the MdmX RING domain. Biochem Biophys Res Commun 2014;447:696–701.
32. Lijnzaad P, Argos P. Hydrophobic patches on protein subunit interfaces: characteristics and prediction. Proteins 1997;28:333–43.
33. Walsh JG, Cullen SP, Sheridan C, Luthi AU, Gerner C, Martin SJ. Executioner caspase-3 and caspase-7 are functionally distinct proteases. Proc Natl Acad Sci U S A 2008;105:12815–9.
34. Menendez D, Inga A, Resnick MA. The expanding universe of p53 targets. Nat Rev Cancer 2009;9:724–37.
35. Hur J, Bell DW, Dean KL, Coser KR, Hilario PC, Okimoto RA, et al. Regulation of expression of BIK proapoptotic protein in human breast cancer cells: p53-dependent induction of BIK mRNA by fulvestrant and proteasomal degradation of BIK protein. Cancer Res 2006;66: 10153–61.
36. Polyak K, Xia Y, Zweier JL, Kinzler KW, Vogelstein B. A model for p53-induced apoptosis. Nature 1997;389:300–5.
37. Bodet L, Menoret E, Descamps G, Pellat-Deceunynck C, Bataille R, Le Gouill S, et al. BH3-only protein Bik is involved in both apoptosis induction and sensitivity to oxidative stress in multiple myeloma. Br J Cancer 2010;103:1808–14.
38. Minsky N, Oren M. The RING domain of Mdm2 mediates histone ubiquitylation and transcriptional repression. Mol Cell 2004;16:631–9.
39. Zhu Y, Regunath K, Jacq X, Prives C. Cisplatin causes cell death via TAB1 regulation of p53/MDM2/MDMX circuitry. Genes Dev 2013;27:1739–51.
40. Mancini F, Moretti F. Mitochondrial MDM4 (MDMX) An unpredicted role in the p53-mediated intrinsic apoptotic pathway. Cell Cycle 2009;8:3854–59.
41. Mancini F, Pieroni L, Monteleone V, Lucà R, Fici L, Luca E, et al. MDM4/HIPK2/p53 cytoplasmic assembly uncovers coordinated repression of molecules with anti-apoptotic activity during early DNA damage response. Oncogene 2015 May 11. [Epub ahead of print].
42. Shi Y, Nikulenkov F, Zawacka-Pankau J, Li H, Gabdoulline R, Xu J, et al. ROS-dependent activation of JNK converts p53 into an efficient inhibitor of oncogenes leading to robust apoptosis. Cell Death Differ 2014;21:612–23.
43. Green DR, Galluzzi L, Kroemer G. Cell biology. Metabolic control of cell death. Science 2014;345:1250256.
44. Trachootham D, Alexandre J, Huang P. Targeting cancer cells by ROS-mediated mechanisms: a radical therapeutic approach? Nat Rev Drug Discov 2009;8:579–91.
45. Hedstrom E, Eriksson S, Zawacka-Pankau J, Arner ES, Selivanova G. p53-dependent inhibition of TrxR1 contributes to the tumor-specific induction of apoptosis by RITA. Cell Cycle 2009;8:3584–91.
46. Ray-Coquard I, Blay JY, Italiano A, Le Cesne A, Penel N, Zhi J, et al. Effect of the MDM2 antagonist RG7112 on the P53 pathway in patients with MDM2-amplified, well-differentiated or dedifferentiated liposarcoma: an exploratory proof-of-mechanism study. Lancet Oncol 2012;13:1133–40.
47. Iancu-Rubin C, Mosoyan G, Glenn K, Gordon RE, Nichols GL, Hoffman R. Activation of p53 by the MDM2 inhibitor RG7112 impairs thrombopoiesis. Exp Hematol 2014;42:137–45.
48. Wu D, Gao Y, Qi Y, Chen L, Ma Y, Li Y. Peptide-based cancer therapy: opportunity and challenge. Cancer Lett 2014;351:13–22.
49. Yang Y, Ludwig RL, Jensen JP, Pierre SA, Medaglia MV, Davydov IV, et al. Small molecule inhibitors of HDM2 ubiquitin ligase activity stabilize and activate p53 in cells. Cancer Cell 2005;7:547–59.
50. Herman AG, Hayano M, Poyurovsky MV, Shimada K, Skouta R, Prives C, et al. Discovery of Mdm2-MdmX E3 ligase inhibitors using a cell-based ubiquitination assay. Cancer Discov 2011;1:312–25.

Published OnlineFirst September 10, 2015; DOI: 10.1158/0008-5472.CAN-15-0439

Cancer Research
The Journal of Cancer Research (1916–1930) | The American Journal of Cancer (1931–1940)

AACR American Association for Cancer Research

Targeting the MDM2/MDM4 Interaction Interface as a Promising Approach for p53 Reactivation Therapy

Marsha Pellegrino, Francesca Mancini, Rossella Lucà, et al.

Cancer Res 2015;75:4560-4572. Published OnlineFirst September 10, 2015.